Pediatr Radiol (2008) 38:1314–1322
DOI 10.1007/s00247-008-1032-5

ORIGINAL ARTICLE

Virtual cardiotomy based on 3-D MRI for preoperative planning in congenital heart disease

Thomas Sangild Sørensen · Philipp Beerbaum · Jesper Mosegaard · Allan Rasmusson · Tobias Schaeffter · Conal Austin · Reza Razavi · Gerald Franz Greil

Received: 16 April 2008 / Revised: 30 July 2008 / Accepted: 28 August 2008 / Published online: 25 October 2008

Abstract
Background Patient-specific preoperative planning in complex congenital heart disease may be greatly facilitated by virtual cardiotomy. Surgeons can perform an unlimited number of surgical incisions on a virtual 3-D reconstruction to evaluate the feasibility of different surgical strategies.
Objective To quantitatively evaluate the quality of the underlying imaging data and the accuracy of the corresponding segmentation, and to qualitatively evaluate the feasibility of virtual cardiotomy.
Materials and methods A whole-heart MRI sequence was applied in 42 children with congenital heart disease (age 3± 3 years, weight 13±9 kg, heart rate 96±21 bpm). Image quality was graded 1–4 (diagnostic image quality ≥2) by two independent blinded observers. In patients with diagnostic image quality the segmentation quality was also graded 1–4 (4 no discrepancies, 1 misleading error).
Results The average image quality score was 2.7 – sufficient for virtual reconstruction in 35 of 38 patients (92%) older than 1 month. Segmentation time was 59± 10 min (average quality score 3.5). Virtual cardiotomy was performed in 19 patients.
Conclusion Accurate virtual reconstructions of patient-specific cardiac anatomy can be produced in less than 1 h from 3-D MRI. The presented work thus introduces a new, clinically feasible noninvasive technique for improved preoperative planning in complex cases of congenital heart disease.

Keywords MRI · Surgical planning · Children

T. S. Sørensen (✉) · A. Rasmusson
Department of Computer Science, University of Aarhus,
Aabogade 34,
8200 Aarhus N, Denmark
e-mail: sangild@cs.au.dk

T. S. Sørensen
Institute of Clinical Medicine, University of Aarhus,
Aarhus, Denmark

P. Beerbaum · T. Schaeffter · R. Razavi · G. F. Greil
Division of Imaging Sciences,
King's College London School of Medicine,
London, UK

P. Beerbaum · R. Razavi · G. F. Greil
Department of Paediatric Cardiology,
Guy's and St. Thomas' Hospital,
London, UK

J. Mosegaard
Alexandra Institute,
Aarhus, Denmark

C. Austin
Department of Cardiothoracic Surgery,
Guy's and St. Thomas' Hospital,
London, UK

Introduction

Paediatric cardiac surgeons are often faced with difficult decision making when potential surgical strategies are evaluated preoperatively in complex congenital heart disease. It can be extremely hard to determine in advance whether highly individual spatial relationships would allow certain procedures to be completed. A novel concept for surgical planning in congenital heart disease, namely virtual cardiotomy and surgical simulation, was recently introduced to address these issues [1, 2]. It was suggested that surgeons make any desired incision in a reconstructed heart of patient-specific morphology to gain access to the present defects using virtual surgical tools and thereby estimate the

feasibility of different correction strategies. An example was published as a movie online in which the feasibility of an intracardiac repair in a patient with double-outlet right ventricle (DORV) is examined [2].

Patient-specific virtual models can, in principle, be built from any imaging modality capable of three-dimensional (3-D) imaging, such as echocardiography, CT or MRI. 3-D echocardiography is emerging, but does not yet offer the desired resolution, coverage, and contrast for fast reconstruction of the entire heart and major vessels. Both CT and MRI, on the other hand, can potentially provide high-resolution 3-D data with excellent contrast between the blood pool and the tissue [3–5]. Since patients with complex congenital heart disease often need repeated surgical interventions and preoperative imaging, MRI is most often preferred over CT due to radiation concerns, as the risk of radiation-induced fatal cancer from paediatric CT is not negligible [6, 7]. Also, the high heart rates present in infants and children can limit the value of intracardiac CT imaging with currently available techniques [8]. Contrast-enhanced MR angiography is used routinely for 3-D imaging of the extracardiac morphology and provides excellent preoperative information using multiplanar reconstruction (MPR), maximal intensity projection (MIP), or volume rendering when only vascular structures are of concern [4, 9]. However, as the acquisition is not triggered to the cardiac cycle it cannot be used to image complex intracardiac relations. Using instead an imaging sequence triggered to a short acquisition window in end diastole [5], virtual models of intracardiac morphology have been presented previously [10], but their precision has never been evaluated in a larger patient study.

Therefore, this study presents a quantitative evaluation of the hypothesis that "accurate 3-D virtual models of the heart and the great vessels in infants and children with congenital heart disease can be reconstructed from 3-D steady-state free-precession (SSFP) MRI of diagnostic quality in clinically acceptable reconstruction times and with limited operator dependency". Moreover, we qualitatively studied the feasibility of virtual cardiotomy in selected cases of complex congenital heart disease.

Materials and methods

Study population

We included in the study all infants and children aged 0–10 years who underwent MRI examinations in a 3-month period at our institution. This corresponded to 42 patients who were enrolled in the study. Echocardiography had been performed in all patients and 32 patients (76%) had already had surgery prior to the MRI examination. The average age of the population was 3 years (range 1 day to nearly 10 years), the average weight was 13 kg (range 3–35 kg), and the average heart rate was 96 bpm (range 60–133 bpm). A wide range of complex congenital heart diseases was present in this group, as summarized in Table 1.

All patients were clinically referred for the MRI examination and informed written consent was obtained from the parents or carers. The local ethics committee approved the study.

Study design

The study included a quantitative evaluation of the MRI quality and the segmentation and reconstruction accuracy. The concept of virtual cardiotomy for preoperative planning was evaluated qualitatively.

For the quantitative study we retrospectively completed the following steps in the specified order.

1. Each 3-D dataset was initially segmented (by T.S.S) without knowledge of the individual diagnosis using commercial software (Cardiac3D; Systematic Software Engineering, Aarhus, Denmark). The exact segmentation time for each dataset was noted.
2. The image quality of each MRI dataset was subsequently rated independently by two MRI-experienced paediatric cardiologists (P.B., G.F.G) according to the classification in Table 2, an adapted version of the scoring system used previously [5]. A distinction between nondiagnostic and diagnostic image quality occurs between grade 1 (nondiagnostic) and grade 2 (diagnostic). To achieve this distinction each observer was asked to perform a blinded and complete sequential morphological analysis [11] from each dataset alone. The result was subsequently compared to the patients' diagnoses obtained from echocardiographic studies, previous surgery and other MRI sequences to determine whether the overall rating of a dataset should be diagnostic (score 2–4) or nondiagnostic (score 1).
3. For all datasets graded with diagnostic image quality (grade 2–4) the observers were subsequently asked to independently evaluate the corresponding segmentation (i.e. the virtual model) according to the classification presented in Table 3. As a full anatomical description of the morphology was obtained from the image data according to the previous classification, the model segmentation should reflect this. For the segmentation classification we consequently distinguished between a misleading segmentation (grade 1) and segmentations with moderate, minor or no discrepancies (grades 2–4, respectively). Each segmentation was presented transparently in colour on top of the original dataset to facilitate an accurate assessment of its quality. Interac-

Table 1 Study population.

No. of patients	Diagnoses	Previous surgery	MRI ≥2 (*n*)[a]	ICP (*n*)[b]	ICS (*n*)[c]
6	Hypoplastic left heart syndrome	Norwood I (*n*=3), Norwood II (*n*=1), Fontan (*n*=1), none (*n*=1)	4	2	
5	AVSD: balanced (*n*=1), balanced with hypoplastic aortic arch (*n*=1), unbalanced (*n*=3)	Repair with residual ASD (*n*=1), none (*n*=1), Norwood II (*n*=2), PA band (*n*=1)	5	5	1
4	TOF (*n*=3), TOF with absent pulmonary valve syndrome (*n*=1)	Repair (*n*=3), none (*n*=1)	4	1	
4	Pulmonary atresia with VSD (*n*=2), without VSD (*n*=2)	MBTS (*n*=3), RV-PA conduit with VSD closure (*n*=1)	3	2	1
4	CoA with VSD (*n*=1), CoA without VSD (*n*=3)	CoA repaired (*n*=2), CoA with VSD left open (*n*=1), native CoA (*n*=1)	4	1	1
2	D-TGA	Repair (*n*=2)	2		
2	DILV, VSD, TGA, hypoplastic RV (*n*=1)	Norwood I (*n*=1), Norwood II (*n*=1)	1	1	
2	Supravalvular aortic stenosis (*n*=1), combined supravalvular aortic and pulmonary stenosis (*n*=1)	Repair (*n*=2)	2		
1	ASD, multiple muscular VSDs	ASD repair, muscular VSDs partially closed	1	1	1
1	Heterotaxy syndrome	Norwood I	1	1	
1	DORV, VSD, D-TGA	PA banding	1	1	1
1	CoA, VSD, supramitral valve membrane, subaortic stenosis	Multistage complete repair	1	1	
1	Absent pulmonary valve syndrome with mitral atresia and VSD	None	1	1	
1	Critical pulmonary stenosis with VSD	Repair	1		
1	TA with double aortic arch, bilateral duct and discontinuous PAs	MBTS with reconstruction of central PAs	0		
1	Right pulmonary vein stenosis	None	0		
1	Double aortic arch	None	1		
1	Cardiac teratoma	None	0		
1	Myocarditis	None	1		
1	Situs solitus with atrioventricular and ventriculoarterial discordance, severe pulmonary stenosis	Fontan	1	1	
1	AVSD, DORV, TGA, pulmonary stenoses	None	1	1	
42			35	19	5

ASD atrial septal defect, *AVSD* atrioventricular septal defect, *CoA* coarctation of the aorta, *D* dextro (right-sided), *DILV* double-inlet left ventricle, *DORV* double-outlet right ventricle, *MBTS* modified Blalock-Taussig shunt, *PA* pulmonary artery, *RV* right ventricle, *TA* tricuspid atresia, *TGA* transposition of the great arteries, *TOF* tetralogy of Fallot, *VSD* ventricular septal defect.

[a] MRI rated as diagnostic quality.

[b] Intracardiac pathology reviewed by the surgeon for assessment of correct intracardiac diagnosis (from the group of patients with diagnostic-quality MRI).

[c] Intracardiac surgery performed after 3-D SSFP MRI and intracardiac anatomy confirmed by the surgeon (from the ICP group only).

tive review of any imaging plane (MPR) as desired by the observers was possible with the software provided.

Cases with surgically relevant intracardiac pathology (ICP; see Table 1) were selected for review by the cardiac surgeon. Various cardiotomies were performed for optimal visualization of the intracardiac morphology. In cases where intracardiac surgery was decided, the surgeon was asked to compare the intracardiac morphology as presented by the surgical simulator with the actual morphology encountered in the operating theatre.

MRI technique

A free-breathing, ECG-triggered, T2-prepared, 3-D SSFP whole-heart MRI sequence with a respiratory navigator [5, 12] was applied closely after contrast-enhanced angiography [4, 9]. The 3-D SSFP MRI sequence has previously been successfully evaluated for operator-independent imaging of adolescents and adults with congenital heart disease [5]. To the best of our knowledge no other MRI technique provides comparable image quality for isotropic 3-D imaging of intracardiac structures.

Table 2 Image quality scoring system (adapted from [5]).

Score	Description	Class
1	Nondiagnostic quality images.	Nondiagnostic
2	Anatomy visible with moderate blurring and/or moderate image artefacts. Able to establish diagnosis.	Diagnostic
3	Minimal blurring and/or localized image artefacts. Good overall quality diagnostic information with definite diagnosis.	Diagnostic
4	Sharply defined borders and excellent quality diagnostic information.	Diagnostic

The 3-D SSFP data were acquired with a five-element cardiac coil during an acquisition window of 50–60 ms at a resolution of 1.3^3 mm^3 isotropic voxels on a 1.5-T whole-body MRI scanner (Philips Medical Systems, Best, NL). Data were either acquired during end-systole (heart rate >75 bpm) or end-diastole (heart rate <75 bpm). The most desirable rest period of the heart was visually assessed by a retrospectively ECG-gated, 2-D cine SSFP sequence with a high temporal resolution of 80 phases. An overview of the 3-D SSFP sequence settings is presented in Table 4.

Data from further MRI acquisitions such as T1-weighted, 3-D black-blood sequences, 2-D cine SSFP images, and contrast-enhanced angiography were acquired and included in the material evaluating the sequential morphological description from the 3-D SSFP. All patients included in the study were under general anaesthesia.

Segmentation technique

A semiautomatic 3-D segmentation approach was applied [10]. It classified the imaging volume into three categories: (1) the blood pool, (2) the myocardium, and (3) everything else. User interaction consisted of:

1. Initially selecting a cube of interest in the imaging volume.
2. Possibly excluding parts of the remaining volume by intensity thresholds.
3. Interactively inserting coloured markers, i.e. blood = red, myocardium = green, and other = background/fully transparent.
4. Manual corrections overriding the computed segmentation.

Table 3 Segmentation quality scoring system.

Score	Description
1	Misleading error; important structures missing or misleading.
2	Moderate discrepancies without misleading error; important structures segmented with limited accuracy.
3	Minor discrepancies; all surgically relevant structures segmented accurately. Some structures of minor importance segmented less accurately.
4	No discrepancies; all structures (i.e. ventricles, atria, major veins and arteries, major trabeculations and papillary muscles) segmented accurately.

Table 4 Isotropic 3-D SSFP MRI protocol.

Parameter	Value
Field of view (mm)	220–350
Acquired isotropic resolution (mm^3)	1.3×1.3×1.3
Number of slices	50–140
Rectangular field of view (%)	80
Number of averages	1
Acquisition window (ms)	50–60
Navigator window (mm)	3
Sensitivity encoding factor	2
Flip angle (degrees)	90
Repetition time (TR)/echo time (TE) (ms)	4.9/2.4

In a hypothetical perfect dataset just a handful of red and green markers would be sufficient to classify the entire blood pool and myocardium. In clinical practice (i.e. a dataset with noise, partial volume effects, and possibly even localized signal void) the process involves inserting multiple markers of each colour. Markers were inserted interactively and the visualization of the current segmentation was updated immediately after insertion of each new marker. Small or hardly distinguishable structures that could not be picked up by this process were segmented manually in each image slice.

For qualitative evaluation of the accuracy of the reconstructed models we implemented an interactive validation tool. It was used to verify each model against any reformatted plane in the underlying imaging volume [13]. Using this tool we were able to determine visually whether the surfaces of the reconstructed endocardium and epicardium corresponded to the desired borders in the imaging data. An example is given in Fig. 1.

Results

Image quality

In 7 patients (mean age 6 months, mean heart rate 115 bpm) of the 42 patients the image quality was classified as nondiagnostic according to Table 2. For the remaining 35 datasets (average patient age 3.5 years) the average image quality score was 2.9 and 3.1 as graded by the two observers. Looking specifically at patients older than 1 month, 35 of 38 datasets (92%) were classified as

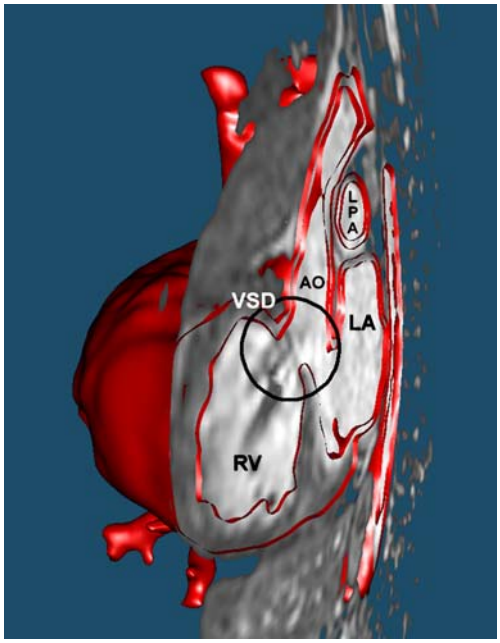

Fig. 1 Interactive validation tool to compare the reconstructed surfaces to the underlying imaging data. The epicardial and endocardial borders cut through the imaging slice, which can be freely selected. An intensity threshold is used to make background voxels fully transparent. The ventricular septal defect (*VSD*) is modelled correctly (*black circle*). The dark area within the right ventricular blood pool (*RV*) is signal void in the MRI volume caused by turbulent flow through the VSD. It was manually segmented as blood. Vessel walls are "grown" automatically from the borders of the blood pool. In this example the wall thickness was exaggerated (note the oblique cut of the lumen of the ascending aorta) but this is fully configurable

diagnostic. The column "MRI ≥2" in Table 1 identifies these datasets. Figure 2 shows an example of the obtained 3-D SSFP MRI quality from a grade-4 quality dataset.

Most of the datasets rated "2" were suffering from localized image artefacts, mainly in the pulmonary arteries. Looking at this group retrospectively, the artefacts are predictable; e.g. in patients with pulmonary artery banding, the turbulent flow resulting from the band caused localized signal void; in patients with a pulmonary artery shunt (e.g. Blalock-Taussig, Norwood I) turbulent flows caused signal void in the shunt itself that partly spread to the pulmonary arteries making them difficult to distinguish clearly. In this group of patients the image quality of the 3-D SSFP datasets seemed to be highly dependent on patients' turbulent flow rates.

Segmentation quality

Figure 2 shows an example of the segmentation quality obtained in one patient. Sagittal, coronal, and transverse imaging planes were reformatted from the isotropic acquisition. The segmentation (blood = red, myocardium = green) is presented transparently for validation with the underlying imaging data. Green and red voxels are present in two shades. The dominant darker shades indicate voxels classified by the marker-driven semiautomatic segmentation algorithm. The brighter green and red voxels on the other hand were drawn manually to correct for errors in the semiautomated process. It is noted that most of the blood pool was found by the marker-driven approach, and only localized corrections such as at the superior vena cava in Fig. 2e were necessary. On the other hand, as indicated by the bright green colours, a significant amount of manual segmentation was required to accurately define the epicardial border. The manual corrections can be applied in any desired imaging plane although only axial planes are shown in Fig. 2.

Figure 3 shows a plot of the segmentation time for each of the 35 patients classified with diagnostic-quality MRI. The segmentation time ranged from 42 min to 85 min with an average of 59 min. The segmentation quality was independently rated by the two observers (P.B., G.F.G) for each patient according to the scoring system in Table 3. The segmentation quality was rated with an average score of 3.5 and 3.6 by the observers. Thus, the observers found only few and mostly unimportant discrepancies between the data and the corresponding segmentation. Typically these discrepancies occurred where the two observers disagreed, at some level, to a subjective aspect of segmentation in an area of poor image signal or contrast.

Virtual cardiotomy

Surgically interesting intracardiac pathology was present in 19 patients in the group of patients with diagnostic image quality (Table 1, column 'ICP'). In six further patients (mean age 1.3 months) examination by virtual cardiotomy would have been feasible but these patients were disqualified due to poor MRI quality hindering accurate reconstruction. Using the virtual cardiotomy simulator, the cardiac segments, the atrioventricular and ventriculoarterial connections, and the present intracardiac defects could be identified and were depicted correctly compared to the available diagnoses. During the study period, cardiac surgery was performed in five patients from this group (see column 'ICS' in Table 1) in which intraoperative findings correlated well with the observations obtained from the virtual models preoperatively. In one patient who underwent surgery for closure of a ventricular septal defect (VSD), a digital photograph of the actual defect was taken during surgery. A comparison of the real morphology to that of the reconstructed model using virtual cardiotomy is presented in Fig. 4. The virtual incision in the right atrium accurately depicts the exact location of the VSD at the root of the aortic outflow tract. The shape of the VSD appears

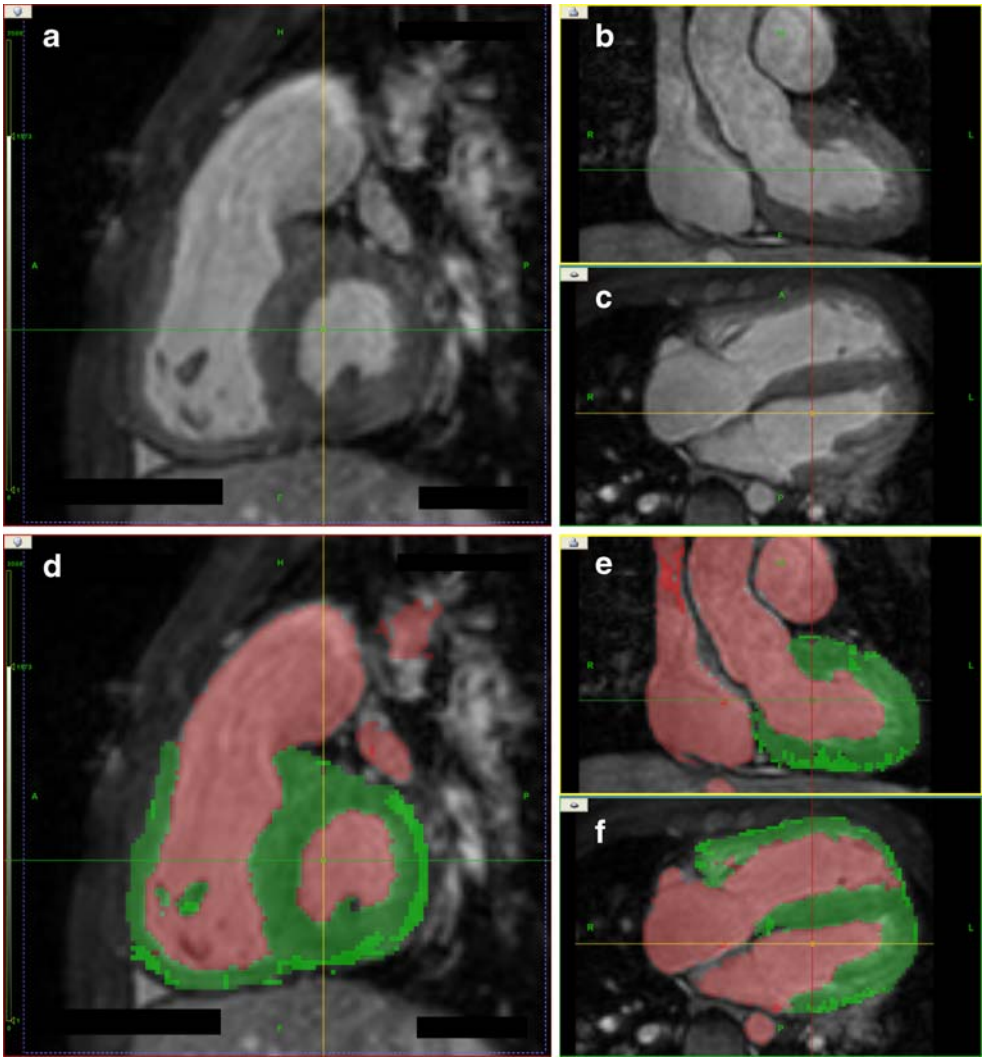

Fig. 2 Isotropic end-systolic 3-D SSFP MRI in a 5-year-old child with surgically repaired tetralogy of Fallot. The raw imaging data are seen at the top (**a**–**c**) and the corresponding segmentation at the bottom (**d**–**f**). Sagittal (**a**, **d**), coronal (**b**, **e**), and transverse (**c**, **f**) planes are shown. The thin yellow, green and red lines depict the intersections between these planes. Red colouring indicates classification of the corresponding voxels to the blood pool, whereas green indicates classification as myocardium. Two shades of green and red are present; the dominant darker shades indicate voxels classified by the marker-driven semiautomated segmentation algorithm, whereas the brighter shades correspond to voxels that were subsequently segmented manually

circular in the reconstruction whereas it appears slightly stretched in the digital photo. This is simply due to deformation by the surgeons' tools. Figure 5 shows an additional example of virtual cardiotomy from the present study. A right ventriculotomy was performed to visualize a VSD. The simulator was used to visualize the size of the (possibly restrictive) VSD in a patient with a hypoplastic right ventricle, double-inlet left ventricle, and transposition of the great arteries. In general, all intracardiac defects, such as VSDs, were easily visualized along with their relationship to other cardiac structures. Finally, in Fig. 6 we made a right ventriculotomy from the aortic root to visualize the spatial relationships of the subaortic outflow tract relative to multiple VSDs to estimate the feasibility of an intracardiac repair in a patient diagnosed with atrioventricular septal defect, DORV, transposition of the great arteries, and valvular and subvalvular pulmonary stenoses.

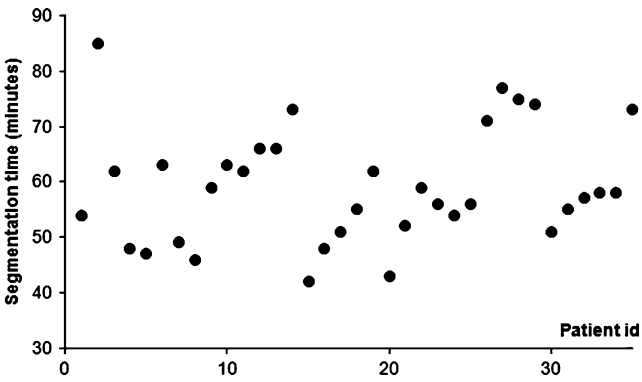

Fig. 3 Segmentation time in minutes for the 35 patients with diagnostic image quality

Discussion

This study evaluated the accuracy of virtually reconstructed morphological models of congenital cardiac defects in a

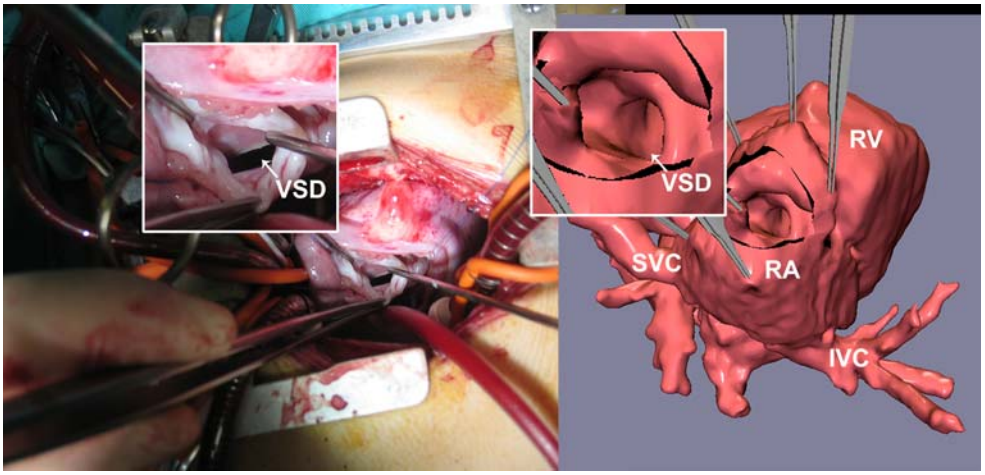

Fig. 4 Surgical image (*left*) and virtual cardiotomy (*right*) in a 1-year-old child with a ventricular septal defect. An incision in the right atrium gives access to the defect, which is located just below the aortic outflow tract. *IVC* inferior vena cava, *RA* right atrium, *RV* right ventricle, *SVC* superior vena cava, *VSD* ventricular septal defect

patient group of 42 neonates, infants and children. Based on the obtained results our hypothesis is now revisited.

The hypothesis stated that "accurate 3-D virtual models of the heart and the great vessels in infants and children with congenital heart disease can be reconstructed from 3-D SSFP MRI data with diagnostic quality in clinically acceptable reconstruction times and with limited operator dependency". As the marker-driven semiautomatic segmentation merely consists of inserting a number of coloured markers in the imaging data, we argue that this can be done mostly operator independently. The user is presented with the current colouring immediately after inserting each new marker and can simply add markers until the desired segmentation is obtained. As there can be no real uncertainty in a dataset rated of good image quality (score 3 or 4), any necessary manual corrections could be performed without ambiguity. Only in data with borderline image quality is significant subjective image interpretation required. Generally speaking, the 3-D data quality improved with the age of the patient and consequent lower heart rate, but could be negatively affected by turbulent flow conditions. As the segmentation quality was generally rated as highly accurate on datasets with diagnostic image quality, and since segmentation times on average were less than 1 hour, we therefore confirm the validity of this hypothesis.

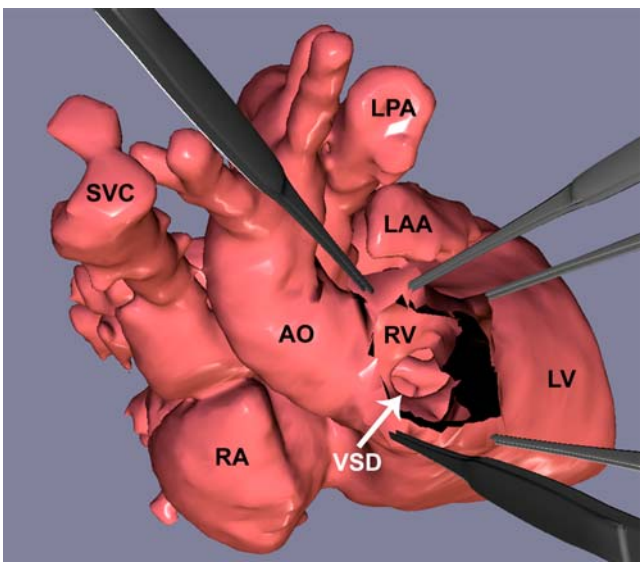

Fig. 5 Virtual cardiotomy in a 4-year-old girl with a hypoplastic right ventricle, double-inlet left ventricle, ventricular septal defect, transposition of the great arteries, and a previous hemi-Fontan operation. An incision is made from the root of the aorta through the rudimentary right ventricle revealing the exact location and size of the VSD. *AO* aorta, *LAA* left atrial appendage, *LPA* left pulmonary artery, *LV* left ventricle, *RA* right atrium, *RV* right ventricle, *SVC* superior vena cava, *VSD* ventricular septal defect

We also qualitatively assessed the feasibility of virtual cardiotomy for preoperative planning. Our study demonstrated that virtual cardiotomy is indeed clinically feasible and a realistic surgical planning option for patients older than 1 month where the diagnostic quality of the underlying MRI image dataset was obtained in 92% of patients. From these reconstructions, surgeons were able to identify the segmental morphology of the intracardiac anatomy using virtual cardiotomy. This leads us to conclude that virtual cardiotomy is a valuable new technique for preoperative planning in children with complex intracardiac anatomy where surgery is particularly difficult due to a limited field of view and complicated access to the site of repair [14]. Using virtual cardiotomy preoperatively it can be ensured that the chosen strategy does in fact provide the desired access for the planned repair. Moreover, as discussed previously [1], virtual cardiotomy could also become a valuable training and educational tool for less-experienced surgeons.

Usually the intracardiac morphology was accurately depicted for precise segmental analysis, whereas certain extracardiac vascular structures were occasionally difficult to delineate, particularly in the presence of turbulent flow. By combining the presented models with reconstructions or

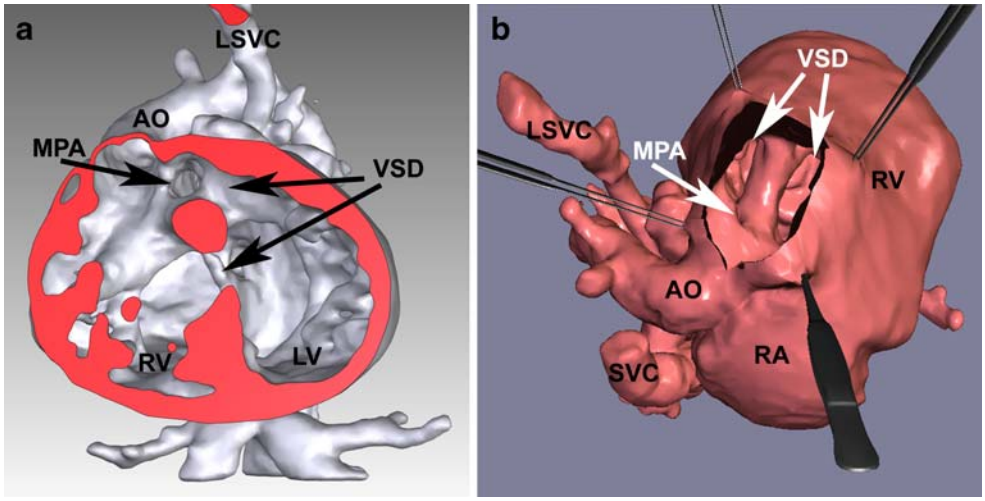

Fig. 6 A 3-year-old girl with complete atrioventricular septal defect, DORV, transposition of the great arteries, valvular and subvalvular pulmonary stenoses, and a left superior vena cava. **a** Virtual reconstruction looking into the right ventricle and left ventricle from the apex, which has been cut away. The outflow tracts of the aorta and main pulmonary artery are visualized relative to the two ventricular septal defects. **b** Virtual cardiotomy; the surgeons' view. An incision is made from the root of the aorta through the right ventricle revealing the exact location and course of the two ventricular septal defects. *AO* aorta, *LSVC* left superior vena cava, *LV* left ventricle, *MPA* main pulmonary artery, *RA* right atrium, *RV* right ventricle, *SVC* superior vena cava, *VSD* ventricular septal defects

volume renderings of contrast-enhanced MR angiography this limitation is expected to be overcome in the future. It is important to note that a fully correct reconstruction is only guaranteed after expert approval of the underlying segmentation of the image data.

The current MRI techniques are limited in 3-D imaging of the atrioventricular or semilunar valves of the heart. This limitation could potentially be overcome by 3-D echocardiography, depending on acoustic windows. However, 3-D echocardiography does not (yet) provide sufficient image quality for 3-D reconstruction of the heart and great vessels due to limited acoustic windows. Further research is required to determine whether a combination of 3-D echocardiographic and 3-D MRI datasets could integrate the cardiac valves in the virtual reconstructions. Multidetector CT (MDCT) on the other hand may be equally as useful as MRI for virtual reconstruction. However, the risks from ionizing radiation are significant, particularly in the paediatric population [6, 7]. For this reason MRI was chosen over MDCT in this study. Moreover, to the best of our knowledge, there is currently no experience available in imaging the cardiac valves in children using MDCT.

Our datasets were acquired during the longest rest period of the heart. For patients with high heart rates this is usually found in end-systole. During cardiac bypass, however, the heart is relaxed and bloodless and its shape is therefore somewhat different from that in our reconstructions. This has not been considered to be a significant disadvantage by the cardiac surgeons. Based on this we believe that despite the difference between systolic and diastolic rest states, 3-D reconstructions can be adapted and used routinely for the most difficult preoperative planning, although further investigations with greater patient numbers would be necessary to prove this hypothesis.

A variety of complex intracardiac malformations exists for which a 3-D reconstruction provides significant supplementary information to the mostly 2-D images otherwise available from the present imaging modalities. One example is patients diagnosed with DORV. The surgeon must estimate whether intracardiac routing of blood from the left ventricle to the aorta through the associated VSD is possible through an intracardiac tunnel, whether it is better to perform a switch operation of the main pulmonary artery and the aorta, or whether to aim for a Fontan repair instead. An illustration is provided in Fig. 6, which presents a useful surgical view to evaluate the feasibility of an intracardiac tunnel in a patient with DORV. A final example is hard-to-access VSDs. Using virtual cardiotomy it is possible to preoperatively evaluate whether a transatrial incision provides the desired access or whether a right ventriculotomy is preferable through either the root of the main pulmonary artery or the apex [15]. In general, the more knowledge the surgeon can obtain of individual spatial relationships (i.e. through virtual cardiotomy), the more likely it is that the strategy that is agreed upon preoperatively can indeed be carried out during surgery.

Limitations

The study focused on the intracardiac anatomy and the presentation of these structures to the cardiac surgeon using the virtual cardiotomy simulator. As a consequence, the

coronary arteries were not segmented for this study even though their course was often well defined with 3-D SSFP MRI. Similarly, arterial shunts (e.g. following a Norwood I procedure) causing signal void in the MRI data were not segmented. As the cardiac valves were not consistently visible in the imaging data no effort was made to include these in the segmentations. Finally, since our models were based on a blood-filled heart they appear somewhat different from the surgical situation with a blood-free relaxed heart on cardiac bypass.

Acknowledgement This work was funded by the Danish Research Council (grant no. 2059-03-0004).

References

1. Sørensen TS, Greil GF, Hansen OK et al (2006) Surgical simulation – a new tool to evaluate surgical incisions in congenital heart disease? Interact Cardiovasc Thorac Surg 5:536–539
2. Sørensen TS, Mosegaard J, Greil GF et al (2007) Images in cardiovascular medicine. Virtual cardiotomy for preoperative planning. Circulation 115:e312
3. Ou P, Celermajer DS, Calcagni G et al (2007) Three-dimensional CT scanning: a new diagnostic modality in congenital heart disease. Heart 93:908–913
4. Geva T, Greil GF, Marshall AC et al (2002) Gadolinium-enhanced 3-dimensional magnetic resonance angiography of pulmonary blood supply in patients with complex pulmonary stenosis or atresia: comparison with X-ray angiography. Circulation 106:473–478
5. Sørensen TS, Korperich H, Greil GF et al (2004) Operator-independent isotropic three-dimensional magnetic resonance imaging for morphology in congenital heart disease: a validation study. Circulation 110:163–169
6. Hollingsworth CL, Yoshizumi TT, Frush DP et al (2007) Pediatric cardiac-gated CT angiography: assessment of radiation dose. AJR 189:12–18
7. Brenner DJ, Hall EJ (2007) Computed tomography – an increasing source of radiation exposure. N Engl J Med 357: 2277–2284
8. Leschka S, Wildermuth S, Boehm T et al (2006) Noninvasive coronary angiography with 64-section CT: effect of average heart rate and heart rate variability on image quality. Radiology 241:378–385
9. Greil GF, Powell AJ, Gildein HP et al (2002) Gadolinium-enhanced three-dimensional magnetic resonance angiography of pulmonary and systemic venous anomalies. J Am Coll Cardiol 39:335–341
10. Sørensen TS, Pedersen EM, Hansen OK et al (2003) Visualization of morphological details in congenitally malformed hearts: virtual three-dimensional reconstruction from magnetic resonance imaging. Cardiol Young 13:451–460
11. van Praagh R (2006) Segmental approach to diagnosis. In: Keane J, Fyler D, Lock, J (eds) NADAS' pediatric cardiology, 2nd edn. Elsevier, Philadelphia, chapter 4
12. Fenchel M, Greil GF, Martirosian P et al (2006) Three-dimensional morphological magnetic resonance imaging in infants and children with congenital heart disease. Pediatr Radiol 36:1265–1272
13. Sørensen TS, Therkildsen SV, Makowski P et al (2001) A new virtual reality approach for planning of cardiac interventions. Artif Intell Med 22:193–214
14. Stellin G, Padalino M, Milanesi O et al (2000) Surgical closure of apical ventricular septal defects through a right ventricular apical infundibulotomy. Ann Thorac Surg 69:597–601
15. van Praagh S, Mayer JE Jr, Berman NB et al (2002) Apical ventricular septal defects: follow-up concerning anatomic and surgical considerations. Ann Thorac Surg 73:48–56